BNL-230319-2026-TECH

Performance Evaluation of Fast Beam Loss Monitor Prototypes for the Electron-Ion Collider

A. Natochii

October 2026

Electron-Ion Collider Project

Brookhaven National Laboratory

U.S. Department of Energy

USDOE Office of Science (SC), Nuclear Physics (NP)

Notice: This technical note has been authored by employees of Brookhaven Science Associates, LLC under Contract No. with the U.S. Department of Energy. The publisher by accepting the technical note for publication acknowledges that the United States Government retains a non-exclusive, paid-up, irrevocable, world-wide license to publish or reproduce the published form of this technical note, or allow others to do so, for United States Government purposes.

DISCLAIMER

This report was prepared as an account of work sponsored by an agency of the United States Government. Neither the United States Government nor any agency thereof, nor any of their employees, nor any of their contractors, subcontractors, or their employees, makes any warranty, express or implied, or assumes any legal liability or responsibility for the accuracy, completeness, or any third party's use or the results of such use of any information, apparatus, product, or process disclosed, or represents that its use would not infringe privately owned rights. Reference herein to any specific commercial product, process, or service by trade name, trademark, manufacturer, or otherwise, does not necessarily constitute or imply its endorsement, recommendation, or favoring by the United States Government or any agency thereof or its contractors or subcontractors. The views and opinions of authors expressed herein do not necessarily state or reflect those of the United States Government or any agency thereof.

Performance Evaluation of Fast Beam Loss Monitor Prototypes for the Electron-Ion Collider

Andrii Natochii,* Evgeny Shulga,† Elke-Caroline Aschenauer, Aleksey Bolotnikov, Erik M. Muller, Julio Renta, Prashanth Shanmuganathan, and Thomas Tsang
Brookhaven National Laboratory, Upton, New York 11973, USA

Bela Urbschat
Graduate School of Science, Nagoya University, Nagoya 464-8602, Japan

(Dated: October 7, 2026)

Reliable beam loss monitoring is essential for machine protection and accelerator diagnostics in the high-intensity Electron-Ion Collider (EIC). To evaluate candidate detector technologies under realistic operating conditions, a dedicated fast beam loss monitoring test stand was installed near the STAR interaction region at the Relativistic Heavy Ion Collider (RHIC). The system simultaneously employed plastic scintillation (CLAWS) detectors, conventional chemical vapor deposition (CVD) diamond detectors, scintillating diamond-powder detectors, and an electro-optic signal transmission system. Detector performance was evaluated during routine p–p, Au–Au, and O–O physics operation through measurements of beam loss rates, correlations with the RHIC ionization-chamber beam loss monitors (BLMs), bunch-by-bunch loss patterns, abort-gap cleaning losses, and beam abort events. Owing to their large active area, the CLAWS detectors exhibited the highest sensitivity and the strongest correlation with the reference RHIC instrumentation, while maintaining low noise, good operational stability, and low deployment cost. Conventional CVD diamond detectors demonstrated fast response and excellent radiation hardness, making them attractive for high-radiation locations despite their lower sensitivity in the tested configuration and higher cost. The scintillating diamond-powder detectors showed promising performance as an inexpensive detector concept, while the electro-optic readout successfully demonstrated analog optical transmission of fast beam loss signals without measurable degradation of detector performance during initial operation. Long-term operation revealed limitations associated with laser stability, motivating further improvements before routine deployment. The results provide quantitative guidance for the selection and deployment of complementary BLM technologies in the EIC Machine Protection System (MPS) and other future high-intensity accelerator facilities.

I. INTRODUCTION

Reliable beam loss monitoring is an essential component of modern high-intensity particle accelerators. BLMs provide continuous information on uncontrolled particle losses, enabling machine protection, beam diagnostics, and optimization of accelerator performance. For future facilities such as the EIC [1] at Brookhaven National Laboratory (BNL), the BLM system must satisfy several challenging requirements, including high sensitivity over a broad dynamic range, fast response suitable for machine protection, radiation hardness, long-term operational stability, and compatibility with the accelerator environment.

The EIC MPS is expected to operate on time scales ranging from individual machine turns to milliseconds, requiring beam loss instrumentation capable of resolving both fast and slowly varying beam conditions. In addition to protecting accelerator components from abnormal beam conditions, the BLM system will provide valuable information for machine tuning, collimation optimization, and background characterization for the experimental detectors. Consequently, the development and validation of candidate detector technologies under realistic accelerator conditions is an important step toward the final EIC instrumentation design.

Several detector technologies have been proposed for fast beam loss monitoring, each providing different advantages in terms of response speed, sensitivity, radiation tolerance, and implementation complexity. Scintillation-based detectors coupled to silicon photomultipliers (SiPMs) have demonstrated sub-nanosecond timing capabilities while maintaining relatively simple and inexpensive readout electronics. Diamond detectors offer excellent radiation hardness, fast charge collection, and wide dynamic range, making them attractive candidates for harsh radiation environments. Conventional gaseous ionization chambers, while considerably slower, remain the standard technology for machine protection systems in many existing accelerators due to their robustness and well-understood performance.

To evaluate these technologies under realistic operating conditions, a dedicated beam loss monitoring test stand was set up near the STAR [2] interaction region of the RHIC [3] at BNL. The stand operated parasitically during routine RHIC 25th physics runs [4] in July 2025 through February 2026 without interfering with accelerator operation. Table summarizes the RHIC operating

* natochii@bnl.gov
† eshulga@bnl.gov

parameters relevant to the studies presented in this paper. Multiple prototype detectors, including plastic scintillation detectors, synthetic chemical vapor deposition (CVD) diamond detectors, and scintillating diamond-powder detectors, were operated simultaneously alongside the existing RHIC ionization-chamber BLM system. Continuous waveform acquisition over several months enabled detailed studies of detector stability, beam-loss rates, timing structure, correlations with accelerator parameters, and response during both normal beam operation and beam abort events.

The RHIC environment provides a particularly valuable test platform because it reproduces many of the operational conditions expected at the EIC, including high stored beam intensities, structured bunch patterns, abort gaps, beam abort sequences, and continuously available accelerator diagnostics. By combining high-speed waveform acquisition with accelerator logging data, the detector response can be studied over time scales ranging from individual nanoseconds to complete accelerator fills.

This paper presents the design of the experimental setup, the data acquisition architecture, and the performance evaluation of the investigated detector technologies. Detector stability, sensitivity, timing resolution, and correlations with established RHIC beam loss monitors are examined during routine operation. Particular attention is given to the reconstruction of the beam loss time structure, identification of collision and abort-gap losses, and characterization of detector response during beam abort events. The results provide important input for the ongoing development of fast beam loss monitoring instrumentation for the EIC while also demonstrating the capabilities and limitations of several candidate detector technologies under realistic accelerator conditions.

II. PERFORMANCE EVALUATION CRITERIA

The EIC MPS requires beam loss monitors capable of reliably detecting abnormal beam losses over a broad range of operating conditions. Since no single detector technology simultaneously optimizes all desired characteristics, several complementary detector concepts were evaluated in this study. Their performance was assessed according to the criteria summarized below.

a. Timing Performance The detector response time is one of the most critical parameters for machine protection. Fast beam losses can develop on timescales comparable to a few accelerator turns; therefore, the detector and associated readout electronics should provide nanosecond-scale signal formation with minimal latency. Fast timing also enables bunch-by-bunch beam loss studies and detailed reconstruction of the temporal structure of beam losses.

b. Sensitivity and Dynamic Range An effective beam loss monitor must be capable of detecting both small continuous beam losses during routine operation and large loss events associated with abnormal machine conditions. The detector should therefore provide sufficient sensitivity while maintaining a sufficiently wide dynamic range to avoid signal saturation during intense beam loss events.

Experience from existing high-energy colliders demonstrates that beam loss monitoring systems may need to accommodate loss rates ranging from approximately 10^9 particles/s to substantially higher localized losses, corresponding to dose rates spanning several orders of magnitude. For example, beam loss monitoring systems at RHIC have been designed to cover loss conditions ranging from approximately 4 rad/s for slow losses to $\sim$ 80 krad/s for fast losses [5], while LHC [6] and SuperKEKB [7] experience similarly broad ranges of beam-loss and radiation conditions.

Preliminary beam-loss studies for the EIC indicate steady-state beam-loss rates at the primary collimators of approximately 10^9 particles/s for the hadron ring and 10^{10} particles/s for the electron ring. Beam losses associated with fast instabilities may be several orders of magnitude higher than these steady-state levels. These estimates provide an initial indication of the signal range that the EIC beam loss monitoring system may need to accommodate. Dedicated beam-loss simulations and cumulative total ionizing dose (TID) calculations are foreseen to quantify the expected loss rates and radiation environment at the detector locations and to establish the final sensitivity, dynamic-range, and radiation-hardness requirements. The results of these studies will be reported separately.

c. Signal-to-Noise Ratio Reliable beam loss measurements require stable detector baselines and low intrinsic noise. High signal-to-noise ratios simplify online discrimination between genuine beam losses and electronic noise, reducing false triggers and improving monitoring reliability.

d. Radiation Hardness Beam loss monitors are continuously exposed to significant radiation doses throughout accelerator operation. Detector materials, photodetectors, and front-end electronics must maintain stable performance over prolonged irradiation while minimizing degradation of sensitivity and timing characteristics.

e. Operational Stability Long-term stability is essential for continuous accelerator operation. Detector gain, baseline, and trigger thresholds should remain stable over weeks to months with minimal maintenance or recalibration. Environmental effects, such as temperature variations or electromagnetic interference, should have limited impact on detector performance.

f. Scalability and System Integration The EIC beam loss monitoring system will ultimately consist of a large number of detectors distributed throughout the accelerator complex. Candidate detector technologies should therefore allow cost-effective mass production, straightforward installation, compact mechanical design, and compatibility with the accelerator timing, controls, and machine protection infrastructure.

TABLE I: RHIC beam parameters during the 2025 physics run relevant to the measurements presented in this work. β^*, L_{peak}, and ε represents the betatron function at the interaction point, peak luminosity, and RMS emittance, respectively.

Species	Collisions at STAR	Operation Period	Energy [GeV/nucleon]	Number of Bunches	Intensity [ions/bunch]	β^* [m]	ε [µm]	L_{peak} (STAR) [$\text{cm}^{-2}\,\text{s}^{-1}$]
Au–Au	Yes	05/31/2025–12/08/2025	100.0	111	2×10^9	0.7	$2.15 \rightarrow 0.55$	90×10^{26}
p–p	No	12/08/2025–01/20/2026	100.2	111	220×10^9	0.85	$2.0 \rightarrow 2.6$	N/A
O–O	Yes	01/31/2026–02/06/2026	100.0	111	14×10^9	0.7	$1.1 \rightarrow 1.3$	72×10^{28}

g. Cost Economic considerations become increasingly important as the number of monitoring locations grows. Besides the detector itself, the overall system cost includes front-end electronics, cabling, power supplies, digitizers, maintenance requirements, and installation complexity. A practical detector technology should provide the required performance while remaining economically scalable to a large distributed monitoring system.

The detector technologies investigated in this work are evaluated qualitatively according to these criteria based on measurements performed under realistic RHIC operating conditions.

III. COLLIDER OVERVIEW

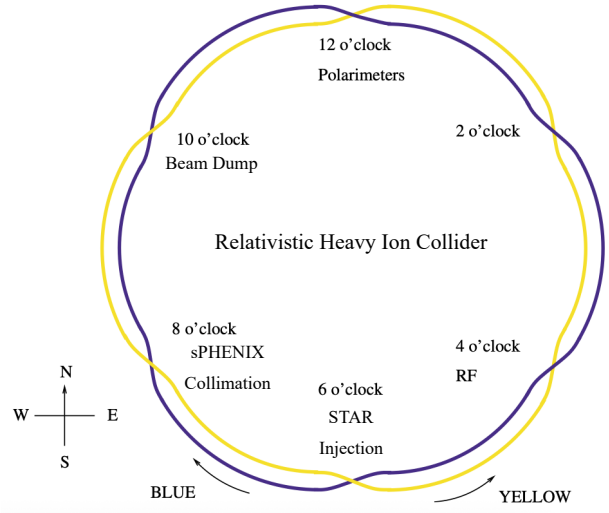


FIG. 1: Schematic drawing of RHIC.

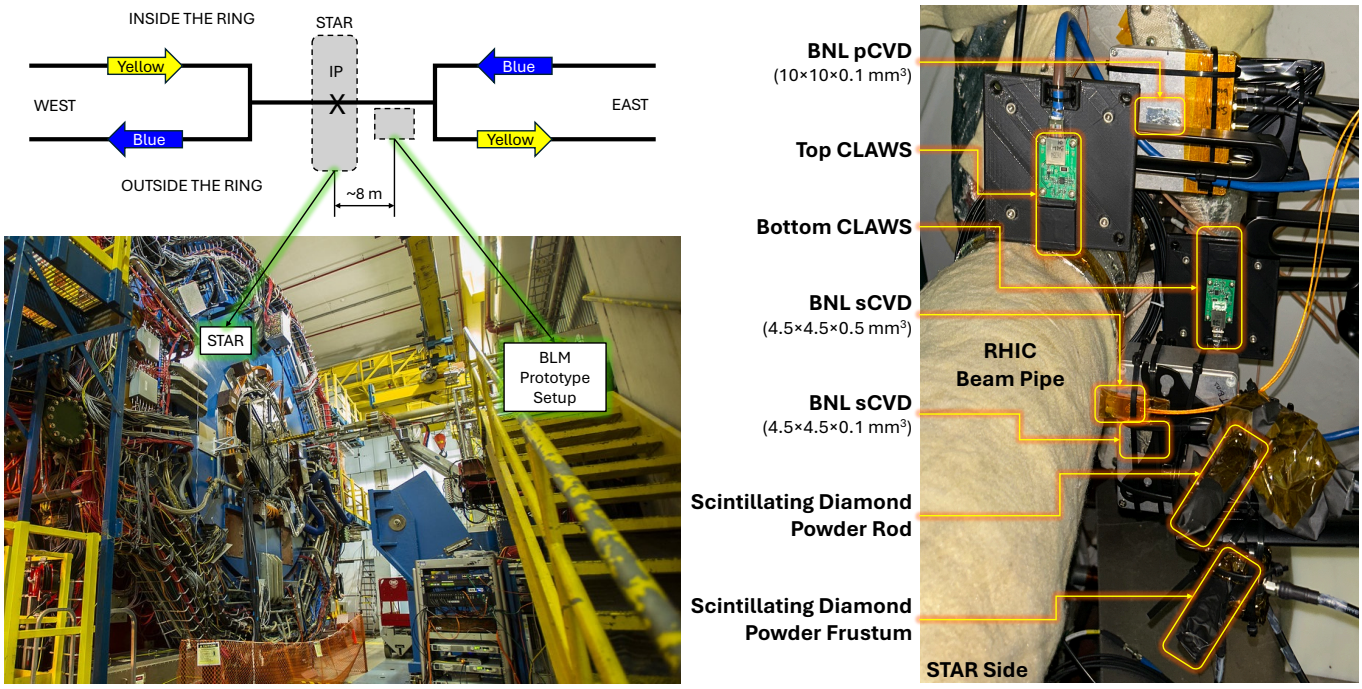
RHIC consists of two superconducting storage rings, referred to as the Blue and Yellow rings, that accelerate and store counter-rotating beams of heavy ions or polarized protons before bringing them into collision at several interaction regions. Figure 1 illustrates the collider schematic drawing. Owing to its operational flexibility, well-developed machine instrumentation, and beam conditions similar to those anticipated for the EIC, RHIC provides an excellent environment for evaluating candidate beam loss monitor technologies.

The detector system was installed near the STAR interaction region, approximately 8 m downstream of the interaction point (IP) along the outgoing beam line, where secondary particles generated by beam losses and collision debris could be measured continuously without interfering with routine accelerator operation. Figure 2 shows the detector location relative to STAR. Figure 2b illustrates the prototype installation assembly around the RHIC beam pipe. The prototype detectors were positioned at radial distances of approximately $\mathcal{O}(10-20\,\text{cm})$ from the beam-pipe center, allowing them to sample the secondary particle field while remaining outside the accelerator vacuum enclosure. Throughout the measurement campaign, the prototype detectors operated parasitically during normal RHIC physics runs, allowing performance evaluation under realistic accelerator conditions including beam injection, acceleration, collisions, beam stores, and beam aborts.

In parallel with the prototype measurements, accelerator operating parameters and beam instrumentation data were continuously recorded using the RHIC control system. These included beam currents, beam energies, luminosity, signals from two adjacent RHIC BLMs [8] based on gaseous ionization chambers, beam emittances, collimator positions, and machine timing events. The ionization-chamber BLMs served as the reference beam loss instrumentation for comparison with the prototype detectors. The synchronized accelerator data enabled detailed correlations between the detector response and machine operating conditions throughout the measurement campaign.

IV. PROTOTYPE BEAM LOSS MONITOR SYSTEMS

To investigate detector technologies suitable for the EIC beam loss monitoring system, several prototype detectors based on different detection principles were evaluated simultaneously at RHIC. The tested technologies included plastic scintillation detectors, synthetic diamond detectors, and scintillating diamond-powder detectors.



(a) (b)

FIG. 2: Experimental setup. (a) Location of the BLM setup near the STAR detector in the 6 o'clock interaction region. (b) Photography of the tested loss monitor prototype setup.

Together these detectors cover a broad range of performance characteristics in terms of timing response, sensitivity, radiation hardness, mechanical complexity, and expected deployment cost. Throughout the measurement campaign, the detector configuration evolved as new prototypes became available or improvements to the readout electronics were implemented. This section describes the operating principles of the investigated detectors and their associated data acquisition systems.

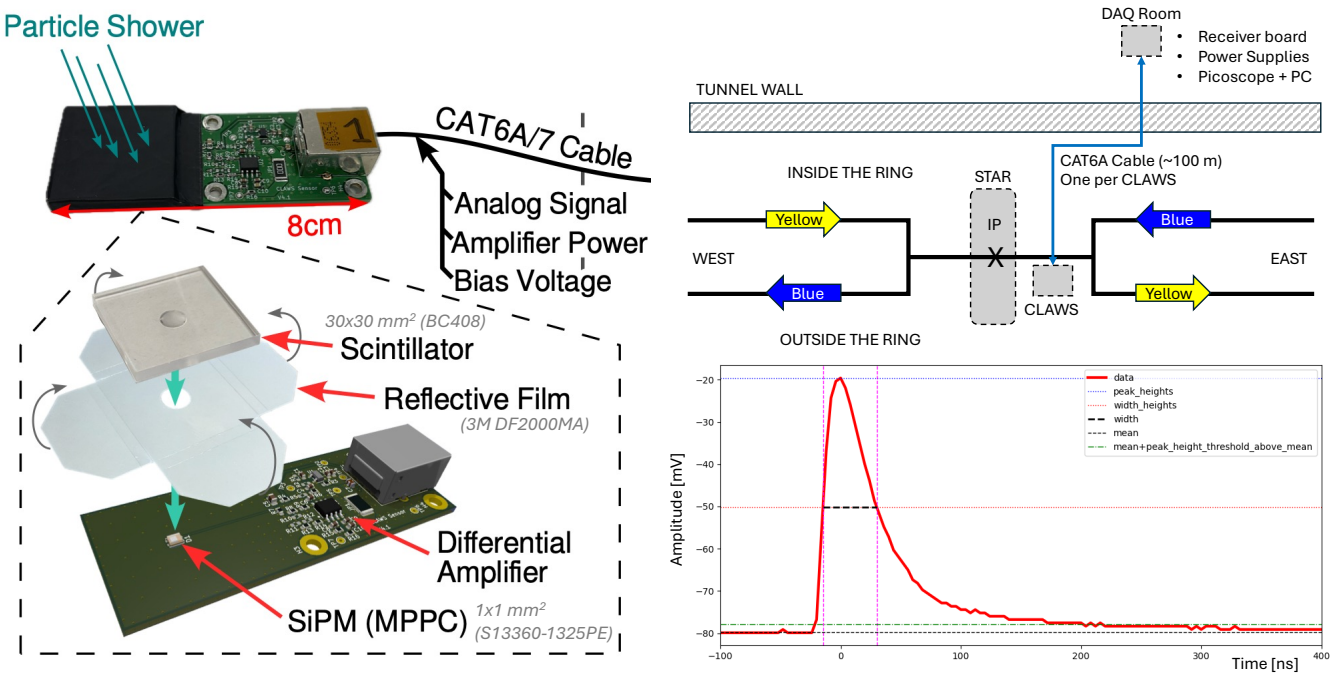
A. Plastic Scintillation Detectors

The primary detector technology investigated in this study was based on the CLAWS (sCintillation Light And Waveform Sensors) detector [9], originally developed at SuperKEKB for fast beam background measurements. Owing to their excellent timing performance, compact design, and relatively low cost, CLAWS detectors are attractive candidates for beam loss monitoring in the Electron-Ion Collider (EIC).

Each CLAWS detector consists of a BC408 plastic scintillator [10] optically coupled to a Hamamatsu S13360-1325PE Multi-Pixel Photon Counter (SiPM) [11]. To maximize light collection efficiency, the scintillator is wrapped in a highly reflective 3M DF2000MA specular reflector film [12]. The detector geometry follows the original CLAWS design developed for the SuperKEKB beam background monitoring system [9]. A photograph and schematic of the detector are shown in Fig. 3a. Charged particles traversing the scintillator produce prompt scintillation light, which is detected by the SiPM and converted into fast electrical pulses. Taking into account the scintillator response, the SiPM characteristics, and the RC shaping of the front-end electronics and long cables, the detector produces output pulses with a characteristic rising time of $\mathcal{O}(10\ \text{ns})$.

The detector readout architecture is illustrated in Fig. 3b. Each CLAWS detector is connected to the data acquisition (DAQ) system located outside the accelerator tunnel via a single approximately 100 m long, shielded CAT6A Ethernet cable, which simultaneously transmits the analog detector signal and supplies the detector with the required low-voltage (± 12 V) power for the front-end electronics together with the high-voltage SiPM bias (typically around 55 V). In the DAQ room, a dedicated receiver board separates the detector signal from the power lines and routes the analog output to a PicoScope 3406D digital oscilloscope [13] for waveform digitization.

The oscilloscope acquired records consisting of approximately 10^8 samples with a sampling interval of 4 ns, corresponding to a continuous observation window of approximately 0.4 s. The 16-bit analog-to-digital converter (ADC) provided 2^{16} amplitude levels over the selected input voltage range. Data acquisition was synchronized to the RHIC revolution timing signal, allowing the temporal structure of beam losses to be reconstructed with respect to the circulating bunch pattern. Following each



(a) (b)

FIG. 3: CLAWS detector setup near STAR at RHIC. (a) Schematic of the detector used in the present study. (b) Detector readout architecture. A representative detector waveform is shown together with its principal pulse characteristics, including the pulse amplitude, rise time, fall time, pulse width, and baseline noise level.

trigger (< 2 ns of jitter RMS), an online peak-finding algorithm extracted the pulse amplitude, width, integral, and arrival time relative to the revolution marker, significantly reducing the stored data volume while preserving the information required for offline analysis. Complete waveform records were periodically archived for validation of the online reconstruction and detailed pulse-shape studies.

B. Diamond-Based Beam Loss Detectors

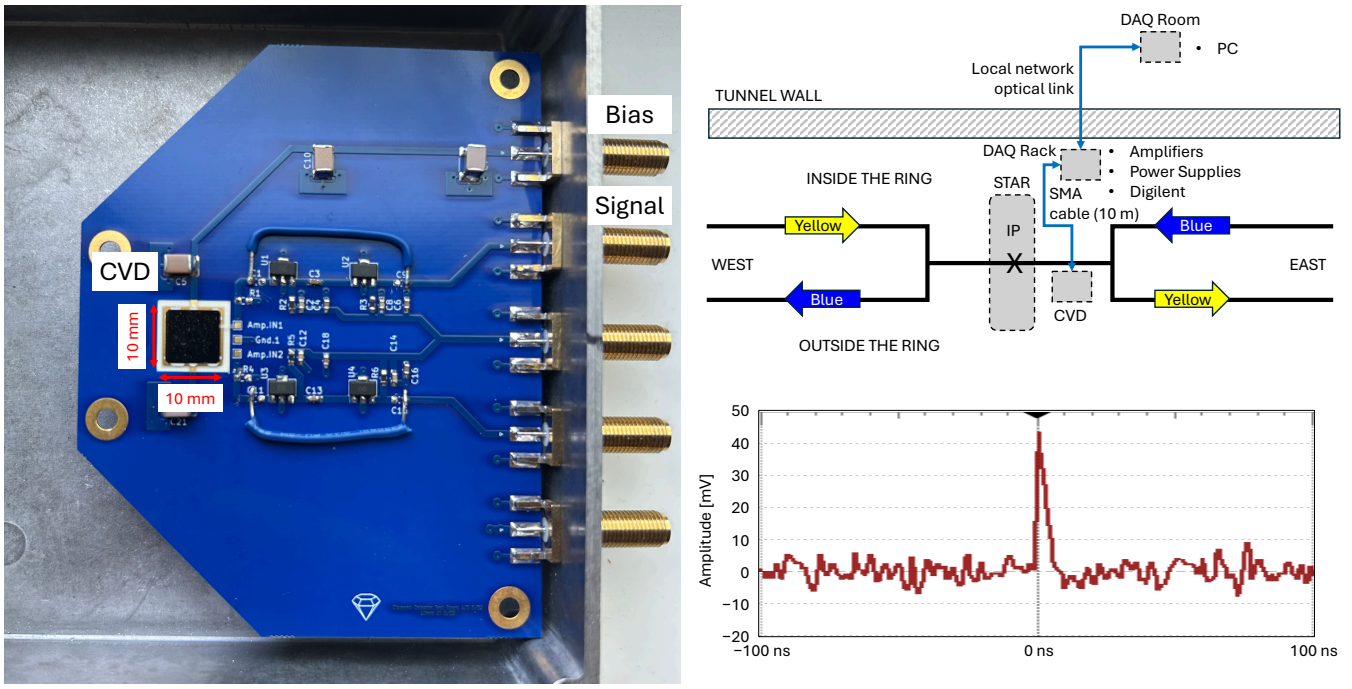
Diamond detectors constitute one of the most promising technologies for future accelerator beam loss monitoring owing to their exceptional radiation hardness, fast charge collection, low leakage current, and wide dynamic range. Several different diamond detector implementations were evaluated during this study.

Initially, measurements were performed using single-crystal chemical vapor deposition (sCVD) diamond detectors fabricated and assembled at BNL. The detector production included metallization and wire bonding of commercially procured diamond substrates, resulting in complete detector assemblies manufactured in-house. Three BNL detector variants were investigated: sCVD diamonds with active dimensions of $4.5 \times 4.5 \times 0.1$ mm^3 at 50 V bias voltage and $4.5 \times 4.5 \times 0.5$ mm^3 at 100 V, and a polycrystalline CVD (pCVD) diamond with dimensions of $10 \times 10 \times 0.1$ mm^3 at 50 V. In addition, a commercially available CIVIDEC B2-HV pCVD diamond detector [14], with dimensions of $10 \times 10 \times 0.5$ mm^3 operated at 500 V, was evaluated for comparison.

Diamond detectors are well suited for beam loss monitoring applications owing to their excellent charge-collection properties, fast signal response, negligible leakage current, and exceptional radiation hardness, remaining operational after accumulated doses of several MGy [15]. These characteristics make them attractive candidates for instrumentation in the harsh radiation environment of modern particle accelerators.

The BNL-fabricated detectors were read out using two low-noise broadband RF amplifiers (Mini-Circuits ZX60-6013E-S+ gain block amplifiers) [16] per detector, whereas the commercial CIVIDEC detector was operated together with the manufacturer-recommended CIVIDEC C2 Broadband Amplifier [17]. The different detector and readout configurations enabled a direct comparison of signal amplitude, noise characteristics, and detection sensitivity under identical beam conditions.

The detector signals were digitized using a four-channel Digilent Analog Discovery Pro ADP5470 mixed-signal oscilloscope [18], providing analog sampling rates of up to 1.5 GS/s. Each acquisition record consisted of approximately 10^6 samples recorded with a sampling interval of approximately 0.67 ns, corresponding to a continuous observation window of about 0.7 ms. The 14-bit analog-to-digital converter (ADC) provided 2^{14} ampli-



(a) (b)

FIG. 4: CVD detector setup near STAR at RHIC. (a) A photograph of the BNL-fabricated diamond detector assembly. (b) Detector readout architecture. A representative CIVIDEC diamond detector (pCVD) waveform is shown.

tude levels over the selected input voltage range. Owing to the relatively low beam loss event rate, the data acquisition system operated in a channel-specific trigger mode, allowing each detector to be monitored independently while recording only waveforms containing valid trigger events. This trigger-based acquisition significantly reduced the stored data volume while preserving the full waveform information for triggered events. When multiple pulses occurred within a single acquisition window, the complete waveform record was stored for detailed offline analysis of the pulse amplitude, timing, pulse shape, and event multiplicity.

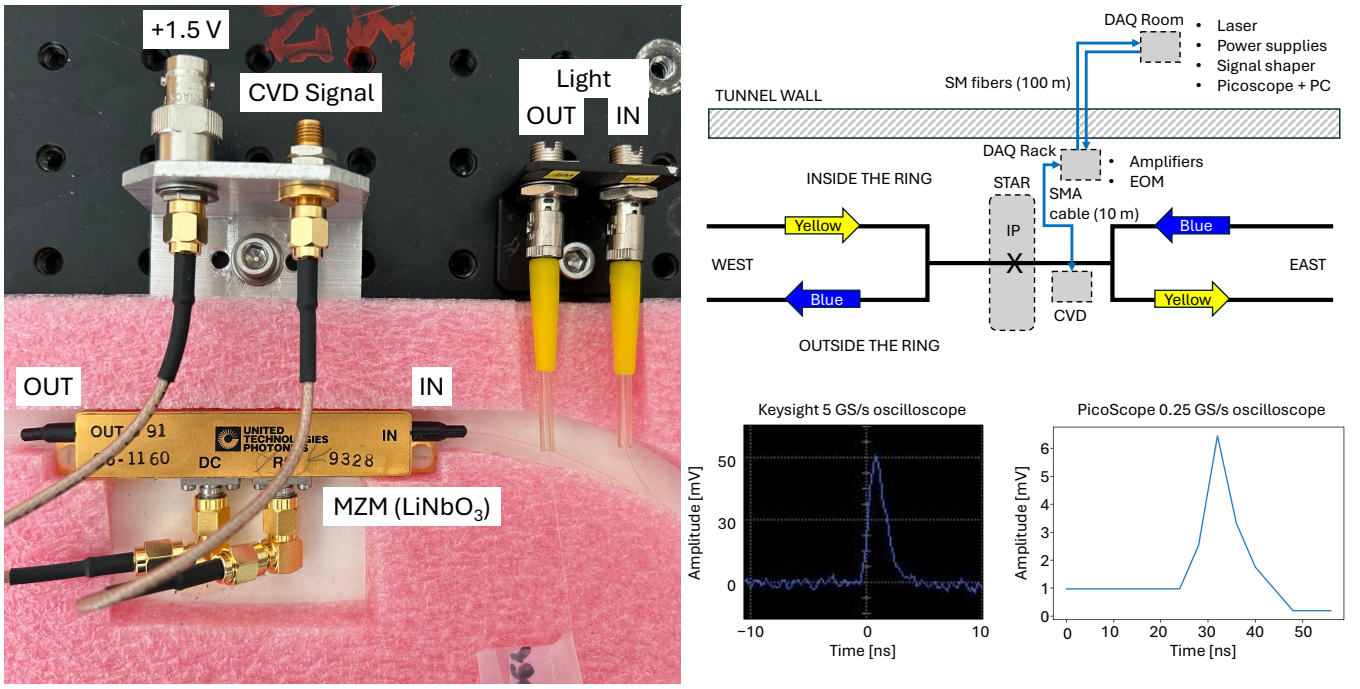
During routine operation, the trigger source was periodically rotated among the detector channels to maximize the number of recorded events for each prototype while maintaining comparable statistics.

A photograph of the BNL-fabricated CVD diamond detector assembly is shown in Fig. 4a, including the metallized diamond sensor, custom readout PCB, wire bonds, SMA signal connector, and mechanical enclosure.

The diamond detector readout architecture is illustrated in Fig. 4b. To preserve the fast detector response and minimize signal degradation, the DAQ electronics were installed inside the RHIC accelerator tunnel approximately 5 m from the detector location. The detector signals were transmitted to the DAQ rack using approximately 10 m long, 3 GHz high-bandwidth SMA coaxial cables, thereby minimizing attenuation and preserving the fast detector signals, characterized by a rise time of approximately 1 ns. The DAQ rack housed the Digilent oscilloscope, broadband amplifiers, detector bias power supplies, and auxiliary electronics required for detector operation. Remote control of the DAQ system was achieved through an operator workstation connected to the Digilent oscilloscope via the local network using optical communication links, enabling continuous detector monitoring and data acquisition without requiring access to the accelerator tunnel during beam operation.

C. Electro-Optic Signal Transmission

One objective of this study was to investigate the feasibility of transmitting beam loss monitor signals optically rather than electrically. In high-energy colliders such as the EIC, fast beam loss signals must be transported over distances of several hundred meters between distributed sensors and their DAQ unit that provides inputs to the MPS while maintaining minimal latency. Since the total response time of the designated fast beam abort system is expected to be limited to approximately four machine turns [19], every component of the machine protection chain, including detector response, front-end electronics, signal transmission, permit logic, and abort kicker triggering, must be carefully optimized to minimize propagation delays. Optical signal transmission offers several potential advantages over conventional electrical links,



(a) (b)

FIG. 5: CVD detector setup near STAR at RHIC. (a) A photograph of the BNL-fabricated diamond detector assembly. (b) Detector readout architecture. A representative BNL-fabricated sCVD $4.5 \times 4.5 \times 0.1$ mm^3 waveform is shown.

including reduced susceptibility to electromagnetic interference, elimination of ground loops, low signal attenuation over long distances, and the possibility of deterministic low-latency communication through optical fibers. Similar latency optimization has been an important aspect of the fast beam abort system developed for SuperKEKB, where significant effort was devoted to minimizing signal propagation delays throughout the protection chain [9].

The present study therefore investigates the use of an electro-optic modulator (EOM) as a proof-of-principle approach for transmitting fast beam loss monitor signals optically. Such a technique could become an important building block of future low-latency beam loss monitoring and machine protection systems at the EIC. Integrated lithium-niobate ($LiNbO_3$) Mach–Zehnder optical intensity modulators (MZMs) have recently emerged as an attractive technology for particle detector readout, offering GHz-level analog bandwidth, excellent linearity, a large dynamic range, and radiation tolerance exceeding 100 Mrad [20]. These characteristics make them particularly well suited for accelerator applications requiring fast analog signal transmission over long distances while preserving both timing and amplitude information.

The electro-optic readout architecture is illustrated in Fig. 5a. Selected BNL-fabricated sCVD detectors were connected to the EOM through approximately 10 m long, 3 GHz high-bandwidth SMA coaxial cables and three low-noise broadband amplifiers. The modulated optical signal was transmitted over a single-mode (SM) optical fiber to the DAQ system, where it was converted back into an electrical signal by a high-speed photoreceiver, processed by signal-shaping electronics, and digitized using PicoScope. A continuous-wave laser operating at a wavelength of approximately 1.3 µm, together with the associated power supplies, was housed in the DAQ room outside of the tunnel.

The MZM operates through the Pockels effect, whereby an applied electric field changes the refractive index of the optical waveguide and consequently modulates the intensity of the laser light propagating through the device. In this way, the fast electrical pulse generated by the diamond detector is converted into an analog optical signal that can be transmitted with minimal attenuation and negligible susceptibility to electromagnetic interference. Figure 5a also includes a photograph of the electro-optic modulator used in this study.

Several detector, amplifier, and modulator configurations were evaluated to characterize the signal fidelity, timing performance, noise characteristics, and bandwidth of the electro-optic transmission chain. Although the electro-optic readout remained at the prototype stage throughout this study, the measurements provide valuable insight into the practical implementation of analog optical signal transmission for future low-latency beam instrumentation and machine protection systems.

D. Scintillating Diamond-Powder Detectors

In addition to conventional solid-state diamond detectors, two prototype scintillating detectors employing synthetic HYPERION diamond-powder [21] dispersed within fused silica (quartz) light guides were built at BNL as discussed in Ref. [22] and investigated. One detector utilized a cylindrical quartz rod, while the second employed a truncated pyramidal (frustum) quartz geometry designed to improve light collection efficiency. The detector assemblies and readout configuration are shown in Fig. 6a.

Unlike charge-collection diamond detectors, these devices operate through scintillation. Secondary particles generated by beam losses produce scintillation photons within the diamond-powder, which are collected and transported through the quartz light guide to a SiPM. In addition, the quartz light guide itself acts as a Cherenkov radiator, generating prompt optical photons from relativistic charged particles traversing the detector that may contribute to the detected signal.

A key advantage of the scintillating diamond-powder detectors is that they generate sufficiently large optical signals to be read out directly by an onsemi MICROFC-SMTPA-60035 SiPM [23] operated at 27 V bias voltage. without the need for external amplifiers, considerably simplifying the front-end electronics compared with conventional charge-collection CVD diamond detectors.

The scintillating diamond-powder detectors represent a potentially inexpensive, mechanically robust, and radiation-tolerant alternative for beam loss monitoring while retaining many of the desirable properties associated with diamond-based sensors. Figure 6b compares representative signals recorded from the conventional CVD diamond detectors and the scintillating diamond-powder detectors using the Digilent data acquisition system. Their performance was evaluated alongside the CLAWS scintillation detectors and conventional diamond detectors throughout the measurement campaign.

V. ROUTINE RHIC OPERATION LOSSES

Prior to discussing the detector performance, it is useful to summarize the origin of the radiation field measured by the prototype beam loss monitors. Since the detectors were installed approximately 8 m from the STAR interaction point, the recorded signals represent a superposition of several beam-induced processes rather than a single localized loss mechanism.

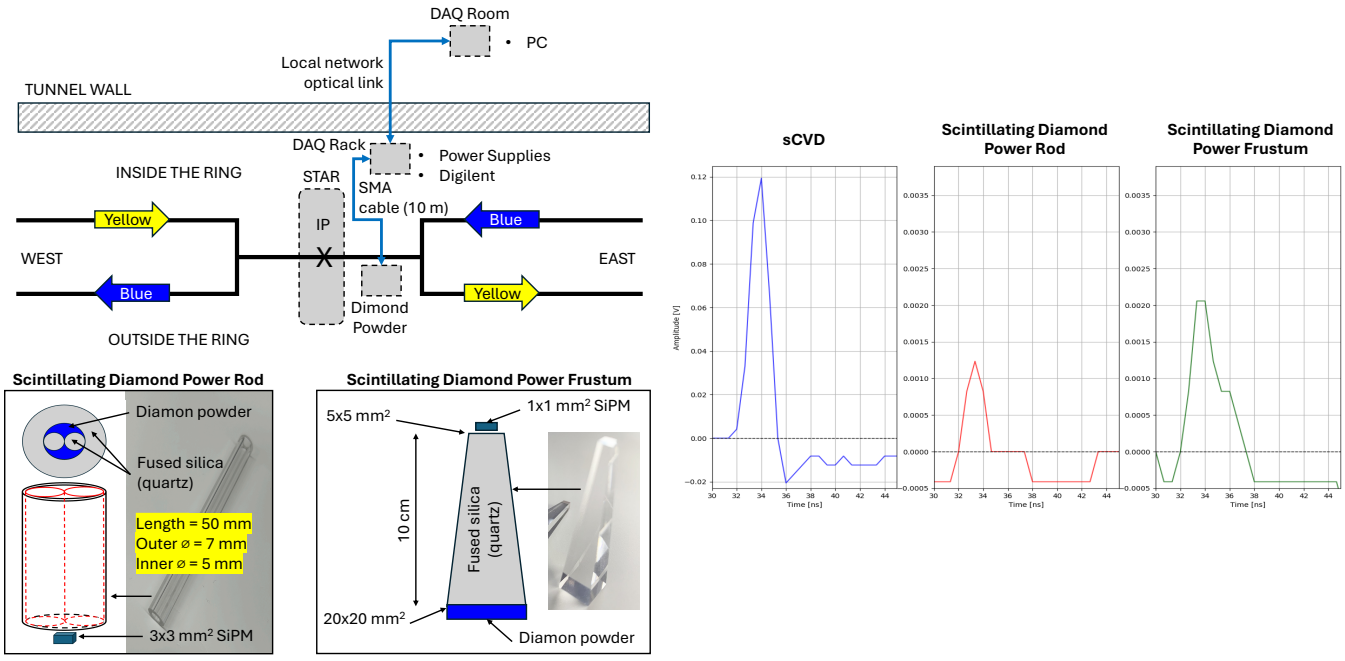
During routine physics operation, the dominant contribution originates from secondary particles produced in beam–beam collisions at the STAR interaction point. Their intensity is therefore closely related to the instantaneous luminosity and gradually decreases during a physics store as the beam currents decay [24]. In addition to collision products, the detectors are exposed to secondary radiation generated by beam halo particles intercepted by the upstream RHIC collimation system installed in the 8 o'clock ring section, which removes particles with large betatron amplitudes before they reach the experimental region [25]. A further contribution arises from beam-gas interactions occurring in the vacuum chamber upstream and around STAR, producing hadronic and electromagnetic showers that propagate toward the detector location. Smaller contributions may also originate from intrabeam scattering, residual beam halo, and occasional local losses associated with orbit corrections or other machine manipulations. Consequently, the measured counting rate should be interpreted as the integrated response to the local radiation environment surrounding the STAR interaction region rather than as a direct measurement of a single beam-loss process. Similar beam-induced background sources have previously been identified in studies of the STAR detector environment [24].

A. Beam Loss Measurements

Figure 7 presents the beam loss rates (i.e., the number of detected signal peaks per second) measured by the prototype detectors during a representative Au–Au physics store at 100 GeV/u. The measured rates gradually decrease throughout the store, reflecting the reduction in beam intensity and instantaneous luminosity. Approximately four hours after the beginning of the fill, a distinct decrease is observed for all detector technologies. This feature coincides with a deliberate 1 mrad change of the horizontal crossing angle implemented to reduce the STAR luminosity [26]. The resulting reduction in collision products decreases the flux of secondary particles reaching the detector location, leading to a simultaneous drop in the signals recorded by both the prototype detectors and the adjacent RHIC ionization-chamber beam loss monitors.

The two CLAWS detectors recorded the highest counting rates among the tested prototypes, ranging from approximately 10-100 kHz. Their signals closely followed the temporal evolution of the RHIC ionization-chamber BLMs throughout the store, demonstrating high detection efficiency and excellent operational stability. In contrast, the CVD and scintillating diamond-powder detectors registered substantially lower counting rates, typically of the order of 1 Hz, owing to their smaller sensitive volumes and the higher trigger thresholds required to suppress electronic noise. Despite these lower absolute rates, all diamond-based detectors reproduced the temporal evolution of the reference BLM system, confirming their ability to reliably monitor relative variations in beam losses.

Overall, all investigated detector technologies operated stably during routine RHIC physics running and responded consistently to changes in accelerator conditions. The strong agreement between the prototype detectors and the established RHIC ionization-chamber BLMs val-



(a) (b)

FIG. 6: Scintillating powder detector setup near STAR at RHIC. (a) Detector readout architecture. (b) A representative BNL-fabricated sCVD $4.5 \times 4.5 \times 0.1$ mm^3 (left), scintillating diamond-powder rod (center), and scintillating diamond-powder frustum (right) waveforms.

idates their capability for monitoring the evolution of beam losses throughout a physics store.

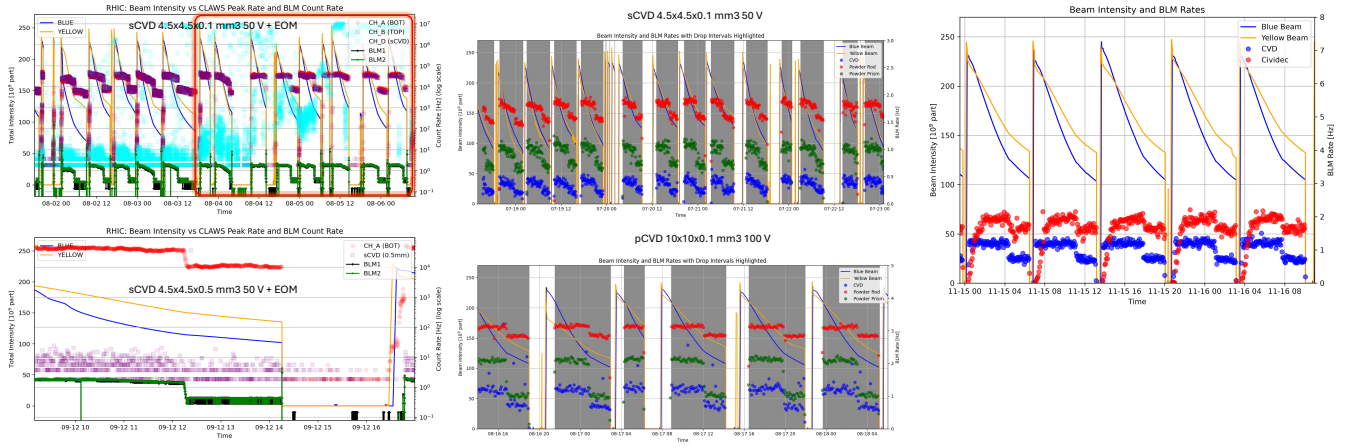
The electro-optic readout operated reliably during the initial period after commissioning and reproduced the beam loss rates measured with the conventional electrical readout without any noticeable degradation in detection efficiency or timing performance. However, after approximately one day of continuous operation, as shown in Fig. 7a and highlighted in red, the system developed significant baseline and counting-rate fluctuations caused by an increase in the relative intensity noise (RIN) of the laser used for optical signal transmission. Stable operation could be restored by periodic adjustment of the laser output power, indicating that the observed instability originated from the optical source rather than from the detector or the EOM itself. These observations demonstrate the feasibility of electro-optic transmission of fast beam-loss signals while also highlighting the need for further optimization of the laser source and optical readout chain to ensure reliable long-term operation.

B. Count Rate Validation

Figure 8 compares the count rates measured by the prototype detectors with those recorded by the adjacent RHIC BLM based on gaseous ionization chambers. For this comparison, the detector rates were synchronized with the RHIC accelerator logging system using common machine timestamps. The prototype count rates were then correlated with the corresponding RHIC BLM measurements over multiple Au–Au physics stores at 100 GeV/u.

The two CLAWS detectors exhibit the strongest correlation with the RHIC BLM system. The measured count rates show an approximately linear dependence on the RHIC BLM signals over the full range of observed beam-loss conditions, confirming that the plastic scintillation detectors accurately reproduce the temporal evolution of beam losses measured by the established RHIC instrumentation.

Owing to their substantially lower count rates ($\sim$ 1 Hz), direct event-by-event correlation between the diamond-based detectors and the RHIC ionization-chamber BLMs is limited by the low counting statistics of both systems. Therefore, the high-rate CLAWS detector was used as the reference detector for evaluating the response of the diamond-based prototypes. As shown in Fig. 8, the single-crystal CVD detector and both scintillating diamond-powder detectors exhibit clear positive correlations with the CLAWS count rate, demonstrating a consistent response to variations in beam-loss conditions throughout the physics stores. Similar correlation quality was observed for all other tested CVD detectors, including both single-crystal and polycrystalline devices. Compared with the CLAWS detector, the diamond-based prototypes exhibit larger statistical fluctuations, primar-



(a) (b) (c)

FIG. 7: Measured beam loss rates during Au–Au collisions at 100 GeV/u at RHIC. The beam intensities in the Yellow and Blue rings are shown by the orange and blue curves, respectively, while the signals from the adjacent RHIC ionization-chamber BLMs are shown by the green and black curves. (a) PicoScope-based DAQ. Top: Bottom CLAWS (red circles), Top CLAWS (magenta squares), and a BNL-fabricated 0.1-mm-thick sCVD detector read out through the EOM system (cyan squares). Bottom: Bottom CLAWS (red circles) and a BNL-fabricated 0.5-mm-thick sCVD detector with the EOM readout (magenta squares). (b) Digilent-based DAQ. Top: BNL-fabricated 0.1-mm-thick sCVD (blue markers), diamond-powder rod (red markers), and diamond-powder frustum (green markers) detectors. Bottom: BNL-fabricated 0.1-mm-thick pCVD (blue markers), diamond-powder rod (red markers), and diamond-powder frustum (green markers) detectors. (c) Digilent-based DAQ. BNL-fabricated 0.1-mm-thick sCVD detector (blue curve) and CIVIDEC pCVD (red curve).

ily due to their smaller sensitive volumes and the higher trigger thresholds required to suppress electronic noise. Among the tested diamond-based detectors, the scintillating diamond-powder frustum exhibits the strongest correlation with the CLAWS detector, while the rod-shaped detector shows somewhat larger scatter.

CIVIDEC detector measurement period was the shortest, thus direct correlation with other detector systems is not illustrative. To see the correlation CIVIDEC detector counts and C-AD BLM count are presented on the bottom of Fig. 8 as a function of time. Time dependence shows similar step structure and follows high counts around 3 am on November 16.

The observed correlations demonstrate that all investigated prototype detectors respond consistently to changes in beam-loss conditions monitored by the RHIC beam loss monitoring system. Although the absolute count rates differ because of variations in detector geometry, sensitive volume, threshold settings, and readout electronics, the approximately linear response confirms that the investigated detector technologies are well suited for monitoring relative variations in beam losses. Among the tested prototypes, the CLAWS detectors provide the highest sensitivity, statistical precision, and operational stability under routine RHIC operating conditions, while the diamond-based detectors offer complementary capabilities, including compact size, excellent radiation hardness, and immunity to electromagnetic interference.

C. Bunch-by-Bunch Loss Pattern

The excellent nanosecond level time resolution of the CLAWS and diamond-based detectors enables the observation of the bunch-by-bunch beam loss structure during routine RHIC operation.

Figure 9a shows the measured loss pattern accumulated over many machine revolutions together with the expected RHIC bunch structure. During Run 25, each RHIC ring was filled with 111 bunches separated by approximately 106 ns, followed by an abort gap of nine empty RF buckets reserved for the beam abort system. The complete beam pattern repeats every revolution period of approximately 12.8 µs.

Three distinct regions can be identified in the measured time distributions: the Blue-ring abort gap (**A**), the collision region (**B**), and the Yellow-ring abort gap (**C**). The collision region consists of a sequence of periodic loss peaks separated by the bunch spacing, corresponding to secondary particles produced by beam–beam

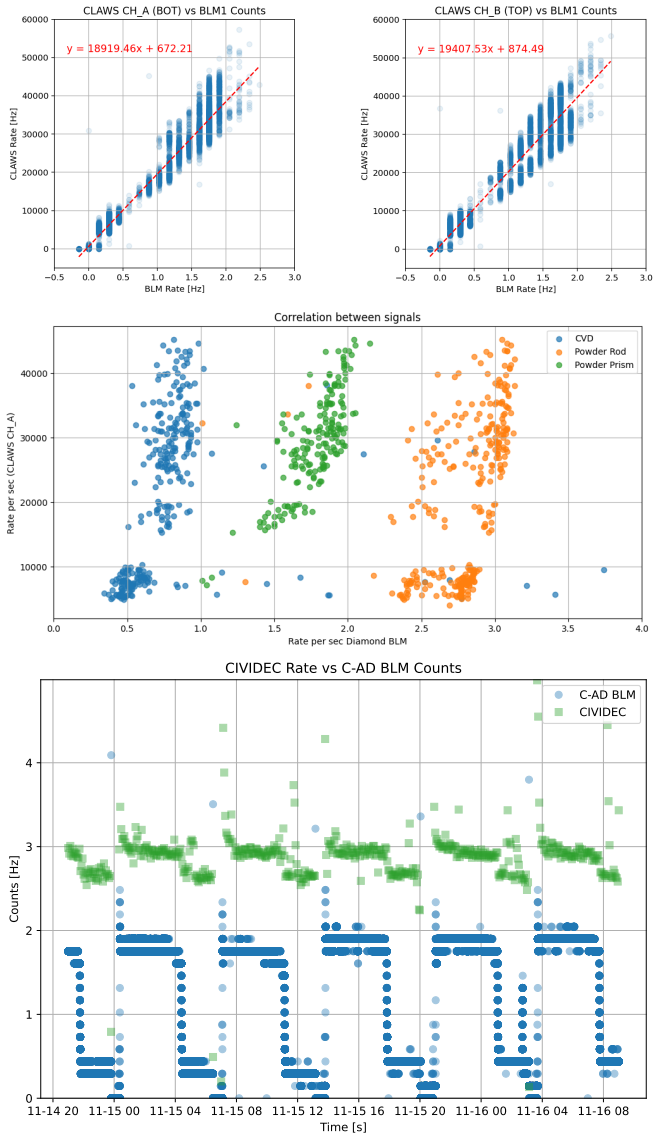


FIG. 8: Correlation between the beam loss count rates measured by the prototype detectors and the reference RHIC ionization-chamber BLM. Top left: Bottom CLAWS detector. Top right: Top CLAWS detector. Center: BNL-fabricated 0.1-mm-thick sCVD detector (blue), scintillating diamond-powder rod detector (orange), and scintillating diamond-powder frustum detector (green). Bottom: CIVIDEC detector (green) and C-AD BLM (blue) as a function of time. The red dashed lines in the CLAWS panels show linear fits; the fitted equations are displayed in the corresponding panels.

collisions at the STAR interaction point. The two abort gaps appear as interruptions in this periodic structure and provide information on single-beam losses originating from the individual RHIC rings. A visible time offset of approximately 400 ns between the CLAWS and Digilent measurements is observed, arising from the difference in the trigger signal path lengths to the two data acquisition systems, which were installed at different locations.

Although the bunch spacing is approximately 106 ns, the measured loss pattern exhibits an additional structure with peaks separated by about 50 ns, as shown in Fig. 9b. This behavior originates from the relative timing of the two counter-propagating beams at the detector location. The Yellow and Blue bunches are synchronized only at the interaction point, where collisions occur. At the beam loss monitor location, approximately 8 m downstream of the interaction point, the two beams arrive at different times because they propagate in opposite directions. Consequently, beam losses associated with the Blue ring appear approximately 50 ns after the collision signal, while the Yellow-ring losses overlap in time with the collision-related peaks. The measured timing agrees with the expected delay determined by the detector position relative to the interaction point and the speed of the circulating beams.

A pronounced asymmetry is observed between the two abort gaps. The Blue-ring abort gap (**A**) contains a distinct beam-loss peak extending over approximately three consecutive bunches, whereas the Yellow-ring abort gap (**C**) exhibits only a nearly uniform background level. Consequently, the Blue-ring single-beam losses measured in the Yellow-ring abort gap are significantly higher than the Yellow-ring losses observed in the Blue-ring abort gap. This asymmetry originates from the RHIC lattice layout and the location of the abort-gap cleaning and collimation system [27, 28]. During heavy-ion operation, a transverse kicker placed in the 2 o'clock region excites debunched particles residing in the abort gap, directing them toward dedicated collimators in the 8 o'clock interaction region for controlled removal. Because the Blue beam passes the STAR interaction region after the abort-gap cleaning system and before reaching collimators, the excited particles produce detectable losses near STAR prior to interception. In contrast, the Yellow beam encounters the abort-gap cleaning system and collimators upstream of STAR, so most of the excited particles are removed before reaching the detector location. As a result, the Blue-ring abort gap exhibits substantially larger single-beam losses than the Yellow-ring abort gap. The collision-related peaks remain the dominant feature of the loss pattern, exceeding the Blue-ring single-beam losses by more than a factor of two, while the single-beam contribution from the Yellow ring is comparatively negligible. This observation is particularly relevant for the EIC, where the RHIC Yellow ring will be reused as the hadron storage ring.

The same bunch-by-bunch loss structure was observed with both the CLAWS and all diamond-based detectors, demonstrating that all investigated technologies provide sufficient time resolution to resolve the RHIC bunch spacing, identify individual abort gaps, and distinguish collision-related losses from single-beam loss mechanisms. These measurements confirm that the prototype detectors are capable of providing bunch-resolved beam loss diagnostics, an important requirement for future machine

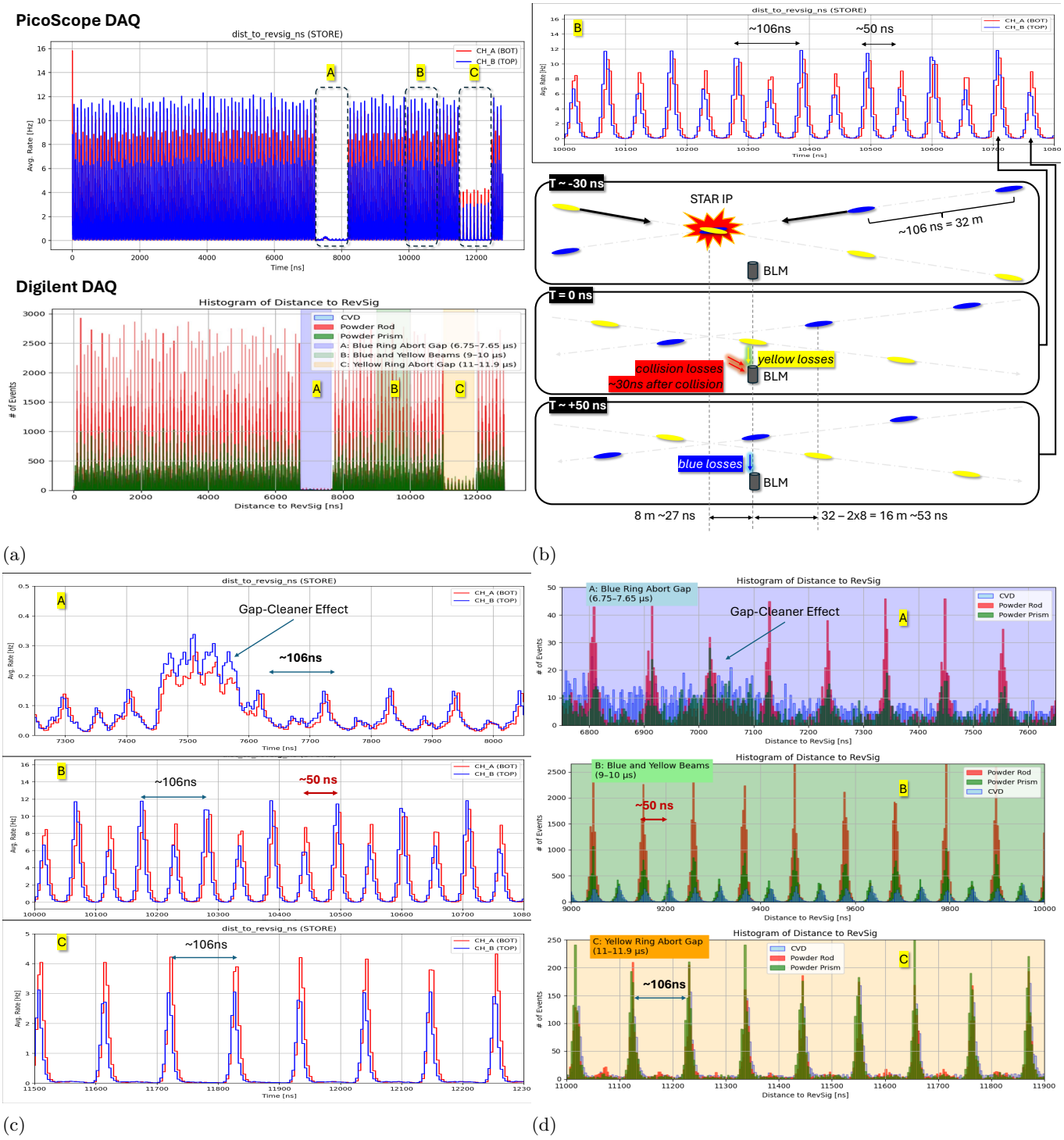


FIG. 9: Measured bunch-by-bunch beam loss pattern during Au–Au collisions at 100 GeV/u at RHIC. (a) Beam loss distribution accumulated over one revolution period, measured with the PicoScope-based (top) and Digilent-based (bottom) DAQ systems. Top: Bottom CLAWS (red) and Top CLAWS (blue) detectors. Bottom: BNL-fabricated 0.1-mm-thick sCVD (blue), scintillating diamond-powder rod (red), and scintillating diamond-powder frustum (green) detectors. (b) Schematic of the beam crossing geometry in the vicinity of the STAR interaction point, illustrating the relative timing of collision- and single-beam loss signals. (c) Expanded view of the beam loss pattern measured with the PicoScope-based DAQ system. (d) Expanded view of the beam loss pattern measured with the Digilent-based DAQ system.

protection and beam diagnostics systems at the EIC.

D. Beam Losses for Different RHIC Beam Species

The final RHIC running period included several beam species and operating conditions, providing a broad range of beam-loss environments for evaluating the prototype detectors. The measurements considered Au–Au and O–O colliding beams, as well as p–p single-beam operation without collisions. The corresponding beam intensity and BLM count rates are shown in Fig. 10 for the three data sets.

A clear correlation between the BLM count rates and the measured beam intensity is observed for all three beam species. In particular, the gradual decrease in beam intensity during each store is accompanied by a corresponding decrease in the BLM rates, demonstrating that the loss monitors reliably follow the evolution of beam losses over the store. The different operating conditions also produce distinct loss-rate patterns, allowing the response and stability of the prototype detectors to be compared over a wide range of beam intensities and loss rates. The count rates measured by the diamond detectors and the CLAWS detector are shown together for direct comparison.

VI. BEAM ABORT MEASUREMENTS

Beam loss monitors are a key component of an accelerator MPS. Their primary function is to detect abnormal beam losses, issue a beam abort request as rapidly as possible, and initiate beam extraction before uncontrolled beam losses can damage accelerator or detector components. Consequently, it is essential that the BLM system remains fully operational throughout the beam abort sequence, accurately recording both the beam losses that trigger the abort request and the transient losses occurring during beam extraction.

During RHIC Run 25, approximately one to two beam aborts were recorded per day. Most aborts were initiated by machine equipment failures, such as power supply trips, rather than by excessive beam losses. The prototype data acquisition systems were configured to continuously record circular waveform buffers, with the trigger positioned near the center of the acquisition window. As a result, each recorded waveform contains approximately equal pre-trigger and post-trigger intervals, allowing the complete beam abort sequence to be analyzed, from the arrival of the trigger signal through beam extraction.

Figure 11 summarizes representative beam abort measurements. The upper panel shows the archived RHIC beam intensities and luminosity during a typical physics store, with the recorded beam abort events indicated by arrows. The lower panels present raw waveforms acquired with the PicoScope-based DAQ system for the Bottom CLAWS detector and the BNL-fabricated 0.5-mm-thick sCVD detector employing the EOM readout. Expanded views of the beam extraction transient are shown on the right.

Beginning in 2021, the RHIC beam abort system was upgraded to mitigate the risk of spontaneous thyratron pre-firing in the abort kicker pulsers by introducing a mechanical relay that delays beam extraction following receipt of the beam abort request [29]. Although this modification significantly improved operational reliability, it introduced an approximately 7 ms delay between the abort request and the actual beam extraction [26]. The prototype detector measurements directly confirm this operational sequence. Following the arrival of the trigger signal (magenta dashed vertical line in Fig. 11, bottom left), beam losses continue at their nominal level for approximately 7 ms, after which the beam is extracted. Immediately after extraction, no further beam-loss activity is observed, confirming the complete removal of both circulating beams. The measured delay agrees well with the expected timing of the upgraded RHIC beam abort system, providing an independent verification of its operation.

The expanded waveforms reveal intense transient beam losses during beam extraction. These loss spikes originate from the finite rise time of the abort kicker magnetic field. During the kicker voltage ramp, particles remaining in the abort gap that were not completely removed by the abort-gap cleaning system [28], together with particles extracted before the kicker reached its nominal field because of imperfect synchronization between the kicker pulse and the abort gap, received only partial deflection. These under-kicked particles continued to circulate for one or more turns before being intercepted by the accelerator aperture or collimation system, producing intense localized beam losses.

The CLAWS detector resolves two distinct loss peaks during beam extraction, corresponding to the sequential passage of the Yellow- and Blue-ring beams through the detector location. The second peak, associated with the Blue ring, exhibits a substantially higher intensity than the first, consistent with the RHIC lattice layout and the locations of the beam abort and collimation systems. The abort kickers for both rings are installed in the 10 o'clock interaction region, whereas the primary collimators are located in the 8 o'clock interaction region. As discussed in the previous section, the Blue beam passes the STAR 6 o'clock interaction region before reaching the collimators and therefore produces larger local losses than the Yellow beam, which encounters the collimation system upstream of STAR.

The sCVD detector equipped with the electro-optic readout records only the larger of the two beam-loss peaks because of its lower detection efficiency compared with the CLAWS detector. Nevertheless, the detector clearly resolves the beam extraction transient, demonstrating that the electro-optic readout preserves the timing information required for fast machine-protection applications.

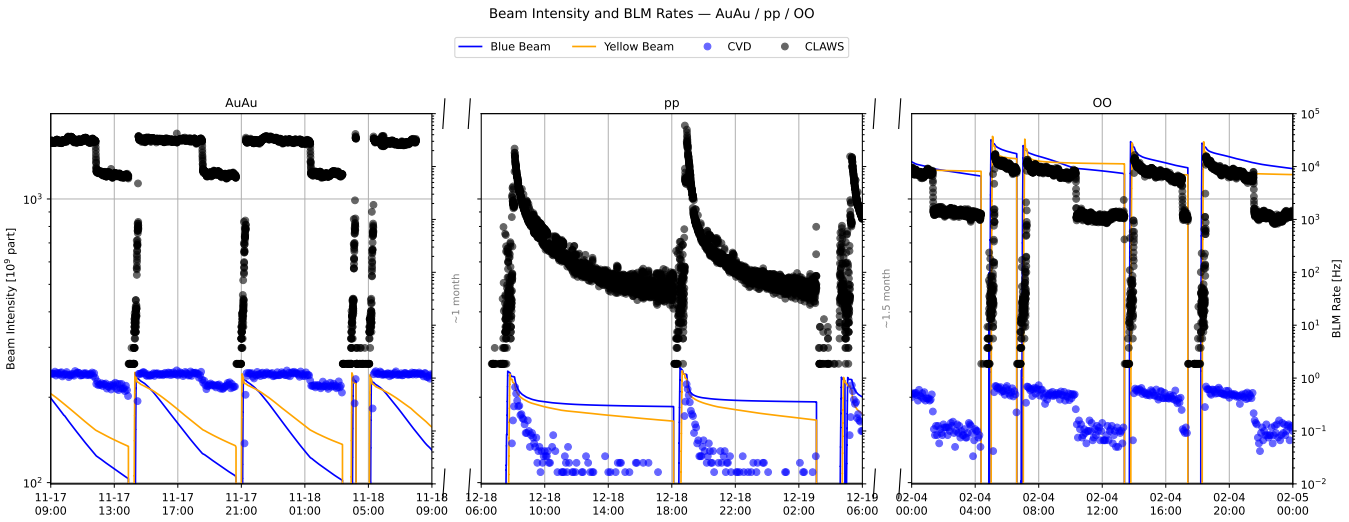


FIG. 10: Comparison of beam loss count rates measured by the prototype detectors during Au–Au and O–O collisions and p–p single-beam operation. The measured beam intensities of the Blue and Yellow beams are shown for reference. Blue: BNL-fabricated 0.1-mm-thick sCVD detector; black: CLAWS channel B.

VII. DISCUSSIONS

The RHIC measurement campaign enabled a direct comparison of several BLM technologies under realistic collider operating conditions, including routine physics stores, bunch-by-bunch beam loss measurements, and beam abort events. Evaluating the prototype detectors according to the criteria defined in Sec. II reveals that each technology offers distinct advantages and limitations, suggesting different application scenarios for the EIC beam loss monitoring system. The radiation exposure accumulated during the campaign also provides a useful reference for assessing the radiation tolerance of the prototype detectors. A recent parasitic detector study performed in the STAR experimental hall during the 2024 RHIC 200 GeV p–p run reported an estimated exposure of approximately 10^{10} 1-MeV neutron-equivalent $(n_{eq})/cm^2$ for a prototype located approximately 8 m from the STAR interaction point on the same platform as the BLM prototypes discussed in this paper, but on the opposite side of the beam pipe [30]. This value was inferred from the radiation-induced increase in the dark current of a reference SiPM and therefore provides a useful benchmark for the radiation environment in the STAR experimental hall, rather than a direct measurement of the dose received by the BLM prototypes. Although the measurements reported here were performed during the 2025–2026 RHIC running periods, including Au–Au, p–p, and O–O collisions, the available radiation estimate provides an indication of the radiation exposure relevant to detectors operating outside the STAR detector. Throughout the measurement campaign, no performance degradation attributable to radiation damage was observed in either the prototype sensors or their signal amplifiers. Thus, the results demonstrate stable operation of the investigated BLM technologies under an extended exposure to the RHIC radiation environment, while the $10^{10} n_{eq}/cm^2$ value should be regarded as an independent reference level rather than as a measured exposure of the prototypes themselves.

Among the investigated detectors, the CLAWS plastic scintillation detector provided the most balanced overall performance. The detector operated reliably throughout the entire measurement campaign without requiring maintenance or recalibration, extending its successful application from the electron-positron environment of SuperKEKB to the hadron collider environment of RHIC. CLAWS exhibited the highest sensitivity, recording beam loss rates of approximately 10-100 kHz, while maintaining a baseline noise below approximately 10 mV. The detector reproduced the reference RHIC ionization-chamber BLM signals with excellent correlation, resolved the bunch-by-bunch beam loss structure, and clearly identified beam abort transients. From an implementation perspective, the detector architecture is particularly attractive because a single approximately 100 m Ethernet cable simultaneously provides power and signal transmission, enabling straightforward installation over large distances. Combined with a sensor cost of approximately $400, these characteristics make the technology well suited for large-scale deployment.

The conventional CVD diamond detectors demonstrated the expected advantages of solid-state beam loss detectors, including fast signal formation, excellent radiation hardness, and compact geometry. The tested detectors successfully resolved the bunch structure and beam abort transients, confirming that their timing performance satisfies the requirements of fast machine protection. Their principal limitation observed during this study was reduced sensitivity to small beam losses, re-

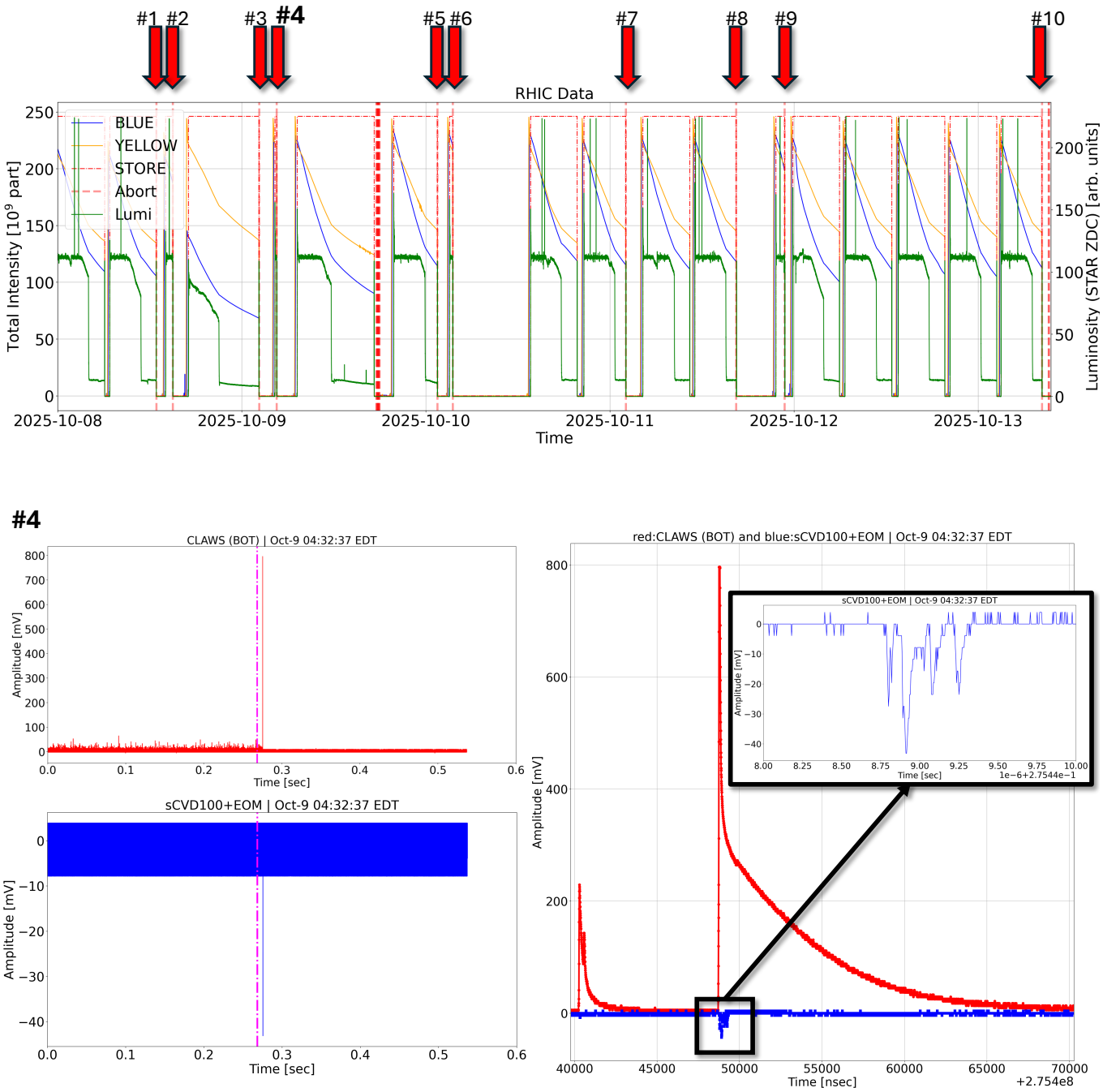


FIG. 11: Representative beam abort measurements during Au–Au collisions at 100 GeV/u at RHIC. Top: RHIC beam intensities and STAR luminosity during a typical physics store. Beam abort events are indicated by arrows. Bottom left: Raw waveform buffers recorded with the PicoScope-based DAQ system for the Bottom CLAWS detector (top, red) and the BNL-fabricated 0.5-mm-thick sCVD detector with the EOM readout (bottom, blue) for one of the recorded abort events (#4). The magenta dashed vertical line indicates the arrival of the trigger signal. Bottom right: Expanded view of the beam extraction transient.

sulting from the relatively small sensitive area (typically below 100 mm^2) and consequently lower counting statistics. The BNL-fabricated detectors exhibited baseline noise of approximately 20-40 mV, whereas the commercial CIVIDEC detector achieved noise levels below 10 mV. Although their sensitivity is lower than that of the CLAWS detectors, this is not expected to be a major limitation for machine protection applications, where the primary objective is reliable detection of abnormal beam losses rather than continuous monitoring of very

small background levels. The principal disadvantage of conventional CVD detectors remains their relatively high cost, typically exceeding $5000 per sensor.

The scintillating diamond-powder detectors demonstrated a promising alternative detector concept. Although the present prototypes produced relatively low counting statistics because of the limited scintillator volume and light collection efficiency, they generated fast signals without requiring external broadband preamplifiers and exhibited clear correlations with the reference detectors. An additional advantage is their very low sensitivity to gamma radiation, which could be beneficial in accelerator regions dominated by electromagnetic backgrounds. Since the detector response is primarily limited by the present optical design rather than the scintillation material itself, improvements in scintillator geometry, powder loading fraction, optical coupling, and SiPM size are expected to substantially increase the light yield. Together with an estimated detector cost of approximately $100, these characteristics justify further development of this technology.

The EOM successfully demonstrated that analog optical transmission can preserve both the timing and beam-loss information of fast CVD detector signals. During the initial period of operation, no measurable degradation of the detector performance or counting rate was observed compared with conventional electrical transmission. However, long-term operation revealed that the stability of the optical readout was limited by the laser source, whose increasing relative intensity noise required periodic adjustment of the optical power. The measurements therefore indicate that the electro-optic transmission concept is technically feasible, although improvements in laser stability and automatic optical power control are required before routine accelerator deployment.

The two evaluated data acquisition systems also exhibited complementary characteristics. The PicoScope-based system provided large continuous acquisition buffers of approximately 0.4 s (4 ns sampling interval, $\sim 10^8$ samples), a flexible software interface, operating-system independence, and convenient long-term operation. In contrast, the Digilent system offered finer temporal sampling (below 1 ns) but was limited to acquisition windows below approximately 10 ms, required a Windows-based software environment, and had a higher system cost (approximately $3500 compared with $2500 for the PicoScope). For continuous accelerator beam loss monitoring, the larger buffer depth and greater operational flexibility of the PicoScope-like architecture appear more advantageous than the additional sampling granularity provided by the Digilent system.

The measurements also provide insight into how different detector technologies could be deployed in the EIC. Rather than relying on a single detector type throughout the accelerator, the results suggest that different technologies are better suited for different radiation environments. Owing to their high sensitivity, low noise, operational stability, simple installation, and relatively low cost, CLAWS detectors appear well suited for widespread installation near sensitive accelerator equipment, where rapid detection of abnormal beam losses is required. Their modest cost also makes replacement straightforward should radiation damage occur after prolonged operation.

Conversely, conventional CVD diamond detectors are particularly attractive for locations expected to experience the highest radiation loads, such as the primary collimation system and interaction regions with the smallest beam apertures. In these locations, the superior radiation hardness and fast response of diamond detectors may outweigh their lower sensitivity and significantly higher cost. The successful operation of both scintillation- and diamond-based detectors under RHIC conditions therefore suggests that a complementary detector layout, rather than a single universal technology, may provide the most effective fast beam loss monitoring solution for the EIC.

VIII. CONCLUSIONS

This work presented the design, deployment, and evaluation of several prototype beam loss monitoring technologies during routine RHIC Run 25 operation. Plastic scintillation (CLAWS), conventional CVD diamond, scintillating diamond-powder, and electro-optic readout systems were operated simultaneously for several months near the STAR interaction region, providing a direct comparison under realistic collider conditions. The measurements demonstrated that the tested detectors could monitor beam losses during routine physics stores, reproduce the temporal evolution of the established RHIC ionization-chamber BLMs, resolve bunch-by-bunch loss structure, identify collision and abort-gap losses, and record fast beam-abort transients.

Among the investigated technologies, the CLAWS detectors provided the highest sensitivity and the best overall combination of stability, timing performance, simplicity, and cost in the tested configuration. Their large active area and low noise make them attractive for distributed beam loss monitoring and for locations where high sensitivity is required. Conventional CVD diamond detectors demonstrated fast response and excellent radiation hardness, supporting their use in high-radiation environments such as collimation systems and interaction regions, although their smaller active area and higher cost resulted in substantially lower counting rates in the present measurements.

The scintillating diamond-powder detectors demonstrated the feasibility of an inexpensive and radiation-tolerant detector concept, but their sensitivity remains limited by the relatively small light yield and active area. Increasing the sensing area and employing multiple SiPMs could improve their detection efficiency and make this approach more competitive for distributed monitoring applications.

The electro-optic readout system successfully demonstrated analog optical transmission of fast beam loss signals without measurable degradation of detector performance during initial operation. However, long-term operation was limited by increasing laser relative-intensity noise and the resulting need for periodic optical-power adjustment. Improved laser stability and, preferably, automatic optical-power control are therefore required before routine accelerator deployment.

Taken together, the results indicate that a single detector technology is unlikely to provide the optimal solution throughout the EIC accelerator complex. Instead, complementary technologies can be selected according to the local radiation environment and monitoring requirements: CLAWS-like scintillation detectors for sensitive and distributed monitoring, CVD diamond detectors for high-radiation locations, and diamond-powder detectors as a potential low-cost option after further optimization. The measurements provide direct experimental input for the selection, placement, and optimization of fast beam loss monitors for the EIC Machine Protection System.

ACKNOWLEDGMENTS

The authors gratefully acknowledge B. Azmoun, W. Betts, I. Blackler, D. Cacace, T. Camarda, D. Gassner, A. Kiselev, T. Kubley, A. Mendez, K. Mernick, A. Ogawa, V. Ptitsyn, M. Purschke, T. Rao, T. Shrey, S. Stoll, T. Throwe, and J. Vasquez (BNL), together with H. Nakayama (KEK), for their invaluable assistance, technical support, fruitful discussions, and for providing materials and equipment essential to this work.

This work was supported by Brookhaven Science Associates, LLC under Contract No. DE-SC0012704 with the U.S. Department of Energy.

[1] F. Willeke and J. Beebe-Wang, Electron Ion Collider Conceptual Design Report 2021, Tech. rep., BNL-221006-2021-FORE; TRN: US2215154 (2021). doi:10.2172/1765663.

[2] K. H. Ackermann *et al.*, STAR detector overview, Nucl. Instrum. Methods Phys. Res. 499 (2-3) (2003) 624–632. doi:10.1016/S0168-9002(02)01960-5.

[3] H. Hahn *et al.*, The RHIC design overview, Nucl. Instrum. Methods Phys. Res. 499 (2) (2003) 245–263. doi:https://doi.org/10.1016/S0168-9002(02)01938-1.
URL https://www.sciencedirect.com/science/article/pii/S0168900202019381

[4] Brookhaven National Laboratory, RHIC Run 25 Overview and Beam Parameters, https://www.agsrhichome.bnl.gov/RHIC/Runs/index.html#Run-25, accessed: July 1, 2026 (2025).

[5] T. J. Shea, R. L. Witkover, RHIC Instrumentation, in: Proceedings of the 1998 Beam Instrumentation Workshop (BIW'98), Vol. 451 of AIP Conference Proceedings, American Institute of Physics, Stanford, CA, USA, 1998, pp. 145–148. doi:10.1063/1.57035.
URL https://www.slac.stanford.edu/pubs/confproc/biw98/shea.pdf

[6] E.B. Holzer *et al.*, Beam Loss Monitoring System for the LHC, Tech. Rep. CERN-AB-2006-009, CERN, Geneva, Switzerland (2006).
URL https://cds.cern.ch/record/930275

[7] S. Bacher *et al.*, Performance of the diamond-based beam-loss monitor system of Belle II, Nucl. Instrum. Methods Phys. Res. 997 (2021) 165157. doi:https://doi.org/10.1016/j.nima.2021.165157.
URL https://www.sciencedirect.com/science/article/pii/S0168900221001418

[8] R. L. Witkover, E. Zitvogel, R. Michnoff, RHIC Beam Loss Monitor System Design, in: Proceedings of the 1997 Particle Accelerator Conference (PAC'97), IEEE, Vancouver, British Columbia, Canada, 1997, pp. 2365–2367.
URL https://cds.cern.ch/record/553724/files/wea168.pdf

[9] K. Yoshihara *et al.*, Development and implementation of advanced beam diagnostic and abort systems in SuperKEKB, Nucl. Instrum. Methods Phys. Res. 1072 (2025) 170117. doi:https://doi.org/10.1016/j.nima.2024.170117.
URL https://www.sciencedirect.com/science/article/pii/S016890022401043X

[10] Y. Liu *et al.*, A Design of Scintillator Tiles Read Out by Surface-Mounted SiPMs for a Future Hadron Calorimeter (2015). arXiv:1512.05900.
URL https://arxiv.org/abs/1512.05900

[11] Hamamatsu Photonics K.K., MPPC (Multi-Pixel Photon Counter) S13360 Series, Hamamatsu Photonics K.K., accessed: July 1, 2026 (2018).
URL https://www.hamamatsu.com/content/dam/hamamatsu-photonics/sites/documents/99_SALES_LIBRARY/ssd/s13360_series_kapd1052e.pdf

[12] 3M, 3M™ Specular Film DF2000MA: Technical Data Sheet, 3M Commercial Solutions Division, revision C (Jan. 2017).
URL https://multimedia.3m.com/mws/media/982449O/3mtm-specular-film-df2000ma-technical-data-sheet.pdf

[13] Pico Technology, PicoScope 3406D USB Oscilloscope, Pico Technology, accessed: July 1, 2026 (2026).
URL https://www.picotech.com/oscilloscope/3000/usb3-oscilloscope-logic-analyzer?kit=3406D

[14] CIVIDEC Instrumentation GmbH, B2-HV pCVD Diamond Beam Loss Detector, https://cividec.at/detectors-B2-HV.html, accessed: 2026-07-02 (2026).

[15] T. Behnke, M. Doucet, N. Ghodbane, A. Imhof, C. Martınez, W. Zeuner, Electromagnetic radiation hardness of diamond detectors, Nucl. Instrum. Methods Phys. Res. 489 (1) (2002) 230–240. doi:https://doi.org/10.1016/S0168-9002(02)00572-7.
URL https://www.sciencedirect.com/science/article/pii/S0168900202005727

[16] Mini-Circuits, ZX60-6013E-S+: Connectorized SMA Linear Gain Block Amplifier, 20 MHz–6000 MHz, Datasheet, https://www.minicircuits.com/pdfs/ZX60-6013E-S+.pdf, revision E, Accessed: 2026-07-02 (2019).

[17] CIVIDEC Instrumentation GmbH, C2 Broadband Amplifier, 2 GHz, 40 dB, https://cividec.at/electronics-C2.html, accessed: 2026-07-02 (2026).

[18] Digilent Inc., Analog Discovery Pro 5000 Series Datasheet, Digilent Inc., accessed: July 2, 2026 (2025).
URL https://files.digilent.com/datasheets/ADP-5000-Series-Datasheet.pdf

[19] A. Natochii, Machine Protection Studies of Fast Instability-Driven Beam Losses in the EIC Electron Storage Ring, Tech. rep., Brookhaven National Lab (June 2026). doi:10.2172/3376117.
URL https://www.osti.gov/biblio/3376117

[20] T. Tsang, V. Radeka, Electro-optical modulators in particle detectors, Rev. Sci. Instrum. 66 (7) (1995) 3844–3854. arXiv:https://pubs.aip.org/aip/rsi/article-pdf/66/7/3844/19006508/3844_1_online.pdf, doi:10.1063/1.1145447.
URL https://doi.org/10.1063/1.1145447

[21] HYPERION Materials & Technologies, Micron Diamond Powders, https://www.hyperionmt.com/en-us/products/Abrasives/micron-diamond/, accessed: 2026-08-13 (2026).

[22] E. M. Muller, A. Bolotnikov, E. R. Farquhar, N. Gallice, T. Tsang, Scintillation properties of diamond powders and feasibility of using them in thermal neutron detectors, Nucl. Instrum. Methods Phys. Res. 1083 (2026) 171093. doi:https://doi.org/10.1016/j.nima.2025.171093.
URL https://www.sciencedirect.com/science/article/pii/S0168900225008952

[23] onsemi, C-Series Silicon Photomultipliers (SiPM), Low-Noise, Blue-Sensitive, onsemi, datasheet, Rev. 6, accessed July 8, 2026 (Nov. 2018).
URL https://www.onsemi.com/pdf/datasheet/microc-series-d.pdf

[24] STAR Collaboration, A Heavy Flavor Tracker for STAR, Tech. Rep. LBL-77347, Lawrence Berkeley National Laboratory, technical Design Report (Aug. 2007).
URL https://www.osti.gov/servlets/purl/939892

[25] R. P. Fliller III, A. Drees, D. Gassner, G. McIntyre, S. Peggs, D. Trbojevic, V. Biryukov, Y. Chesnokov, V. Terekhov, RHIC Collimator Performance, in: Proceedings of the 8th European Particle Accelerator Conference (EPAC'02), JACoW, Paris, France, 2002, pp. 2673–2675.
URL https://proceedings.jacow.org/e02/PAPERS/TUPDO035.pdf

[26] T. Shrey *et al.*, Rhic au-au operation at 100 gev in run 25, in: Proceedings of the 17th International Particle Accelerator Conference (IPAC'26), JACoW Publishing, Deauville, France, 2026, pp. 2239–2241. doi:10.18429/JACoW-IPAC2026-WEP1301.
URL https://www.ipac26.org/prepress/pdf/WEP1301.pdf

[27] A. Drees, L. Ahrens, R. F. III, W. Fu, G. Heppner, V. Kain, Abort Gap Studies and Cleaning During RHIC Heavy Ion Operation, in: Proceedings of the 2003 Particle Accelerator Conference (PAC'03), IEEE, Portland, OR, USA, 2003, pp. 1685–1687. doi:10.1109/PAC.2003.1288636.
URL https://ieeexplore.ieee.org/document/1288636

[28] A. Drees, R. F. III, W. Fu, R. Michnoff, Continuous Abort Gap Cleaning at RHIC, in: Proceedings of the 9th European Particle Accelerator Conference (EPAC 2004), JACoW, Lucerne, Switzerland, 2004, pp. 908–910.
URL https://proceedings.jacow.org/e04/PAPERS/MOPLT162.PDF

[29] M. Valette, A. Drees, L. Ahrens, T. Satogata, W. Fischer, RHIC Machine Protection System Upgrades, in: Proceedings of the 13th International Particle Accelerator Conference (IPAC'22), JACoW Publishing, Bangkok, Thailand, 2022, pp. 3897–3900. doi:10.18429/JACoW-IPAC2022-THPOST048.
URL https://proceedings.jacow.org/ipac2022/papers/thpost048.pdf

[30] W. Zhang *et al.*, First-ever deployment of a SiPM-on-tile calorimeter in a collider: a parasitic test with 200 GeV p p collisions at RHIC, J. Instrum. 20 (06) (2025) P06029. doi:10.1088/1748-0221/20/06/P06029.
URL https://doi.org/10.1088/1748-0221/20/06/P06029